Hybrid magnetic graphitic nanocomposites towards catalytic wet peroxide oxidation of the liquid effluent from a mechanical biological treatment plant for municipal solid waste

Rui S. Ribeiro[a,b], Raquel O. Rodrigues[a,b], Adrián M.T. Silva[b], Pedro B. Tavares[c], Ana M.C. Carvalho[d], José L. Figueiredo[b], Joaquim L. Faria[b], Helder T. Gomes[a,*]

[a] *Laboratory of Separation and Reaction Engineering - Laboratory of Catalysis and Materials (LSRE-LCM), Escola Superior de Tecnologia e Gestão, Instituto Politécnico de Bragança, Campus de Santa Apolónia, 5300-253 Bragança, Portugal.*

[b] *Laboratory of Separation and Reaction Engineering - Laboratory of Catalysis and Materials (LSRE-LCM), Faculdade de Engenharia, Universidade do Porto, Rua Dr. Roberto Frias, 4200-465 Porto, Portugal.*

[c] *CQVR – Centro de Química - Vila Real, Universidade de Trás-os-Montes e Alto Douro, 5000-801 Vila Real, Portugal.*

[d] *Resíduos do Nordeste, EIM, Rua Fundação Calouste Gulbenkian, 5370-340 Mirandela, Portugal.*

*Corresponding author. Tel.: +351 273 303 110; Fax: +351 273 313 051.

E-mail address: htgomes@ipb.pt

This article has been accepted for publication and undergone full peer review.
Please cite this article as DOI: 10.1016/j.apcatb.2017.08.013

Abstract

Magnetite, nickel and cobalt ferrites were prepared and encapsulated within graphitic shells, resulting in three hybrid magnetic graphitic nanocomposites. Screening experiments with a 4-nitrophenol aqueous model system (5 g L^{-1}) allowed to select the best performing catalyst, which was object of additional studies with the liquid effluent resulting from a mechanical biological treatment plant for municipal solid waste. Due to its high content in bicarbonates (14,350 mg L^{-1}) and chlorides (2,833 mg L^{-1}), controlling the initial pH was a crucial step to maximize the performance of the catalytic wet peroxide oxidation (CWPO) treatment. The catalyst load was 0.5 g L^{-1}, a very low dosage when compared to the high chemical oxygen demand (COD) of the effluent – 9,206 mg L^{-1}. At the optimum operating pH (i.e., pH = 6), ca. 95% of the aromaticity was converted and ca. 55% of COD and total organic carbon (TOC) of the liquid effluent was removed. The biodegradability of the liquid effluent was enhanced during the treatment by CWPO, as reflected by the 2-fold increase of the five-day biochemical oxygen demand (BOD_5) to COD ratio (BOD_5/COD), namely from 0.21 (indicating non-biodegradability) to 0.42 (suggesting biodegradability of the treated wastewater). In addition, the treated water revealed no toxicity against selected bacteria.

Lastly, a magnetic separation system was designed for in-situ catalyst recovery after the CWPO reaction stage. The high catalyst stability was demonstrated through five reaction/separation sequential experiments in the same vessel with consecutive catalyst reuse.

***Keywords*:** Core-shell nanocomposites; Heterogeneous Fenton-like process; Mechanical biological treatment; Process water; Magnetic separation.

1. Introduction

The organic fraction accounts for about 30 – 40 wt.% of the municipal solid waste (MSW) produced in Europe, corresponding to over 70 million tonnes per year [1]. A significant portion of this biodegradable waste ends up in landfills [1]; however, this approach is not really sustainable [2]. In order to limit the environmental impact of direct landfill disposal, the EU Directive on waste landfilling (Council Directive 99/31/EC) aims to reduce the biodegradable MSW going to landfills, namely 65 wt.% within just 15 years [3]. As a consequence, the concept of hierarchical waste management is well-established nowadays, mechanical biological treatment (MBT) plants being a suitable alternative that is growing in popularity in many European countries as well as in other countries worldwide [4, 5].

MBT plants typically operate in two steps: the first step comprises residue preparation and sorting into different fractions using mechanical means; the second step envisages the biological treatment of the organic fraction of MSW to produce a stabilised solid output for agronomical applications (compost) or ultimately for disposal to landfill [6]. Under this context, anaerobic digestion is an energy efficient biological treatment technique that allows using the organic fraction of MSW as renewable energy source (e.g. through biogas production) while reducing the environmental impact of its direct landfill disposal [2, 7]. Therefore, MBT plants allow reducing the waste stream going to landfill while benefiting from resources (e.g. recyclables and compost) and energy recovery [5].

In order to achieve optimum process conditions, the biodegradable fraction of the MSW going to anaerobic digestion must first be suspended in, or moistened with water, leading to significant freshwater requirements – from 0.4 to 0.6 m^3 per tonne of waste, for dry or wet fermentation, respectively [7]. In addition to the process water from (i) anaerobic digestion, the other main sources of process water streams are: (ii) leachate from intensive rotting, (iii) pressing water from digestate dewatering and (iv) condensates and/or scrubber water from the exhaust treatment [7]. However, unlike the gaseous emissions and the stabilized solid output,

the literature lacks on information regarding the characteristics and subsequent treatment of the liquid effluent with high pollutant loads resulting from the process water streams of MBT plants for MSW [7].

Bearing this in mind, a liquid effluent was collected from a MBT plant located in the Northeast region of Portugal (currently processing 50,000 tonnes of MSW per year); after detailed characterization, catalytic wet peroxide oxidation (CWPO) – a promising alternative technology to the conventional homogeneous Fenton process [8] – was studied under atmospheric pressure and moderate temperature (80 ^{o}C) for the treatment of this liquid effluent presenting low biodegradability. This approach is in line with the current trend for the intensification of CWPO processes, which is moving the process towards the application of higher temperatures, ranging from 80 ºC to 125 ºC [9-11].

Catalyst design plays a crucial role in CWPO, since this water treatment technology relies on the catalytic decomposition of hydrogen peroxide (H_2O_2) via formation of hydroxyl radicals ($HO^{\bullet}$) – which are very powerful and effective oxidants for the destruction of a huge range of organic pollutants [12, 13]. This is confirmed by several recent review articles on the synthesis and application of heterogeneous metal/magnetic phases in CWPO, either directly applied as catalysts or included in very distinct support/hybrid materials [8, 13-21]. Under this context, our previous work has been mainly focused on the combination of active and magnetically separable iron-based materials with the easily tuned properties of carbon-based materials [14]. As a result, the outstanding performance of a hybrid magnetic graphitic nanocomposite (MGNC) catalyst – composed by a magnetite (Fe_3O_4) core and a graphitic shell – was reported when applied in the CWPO of a typical refractory organic model pollutant (4-nitrophenol; 4-NP) with high load (5 g L^{-1}, corresponding to a total organic carbon content similar to that of the liquid effluent considered in this work) [9]. Specifically, it was concluded that the performance of bare Fe_3O_4 in CWPO is enhanced when this magnetic material is encapsulated within a graphitic structure during the synthesis of MGNC, due to the increased adsorptive

interactions between the carbon phase and the pollutant molecules; while at the same time, the leaching of Fe species from Fe_3O_4 to the treated water is strongly limited due to the confinement effect caused by the carbon shell [9].

Seeking for a MGNC catalyst optimization based on the magnetic core, nickel ferrite ($NiFe_2O_4$) and cobalt ferrite ($CoFe_2O_4$) were prepared in the present work and then encapsulated within graphitic shells, in addition to Fe_3O_4. Due to the easier manipulation, simplicity and increased reproducibility of the experimental results, the 4-NP aqueous model system (5 g L^{-1}) was used for the initial screening of the MGNC catalysts, as well as for the development of an in-situ magnetic separation system for catalyst recovery after the CWPO reaction stage. Afterwards, the MGNC catalyst with higher activity for the CWPO of 4-NP was employed in the treatment of the liquid effluent collected from a MBT plant. The performance of the CWPO process was thoroughly evaluated by systematic measurements of chemical oxygen demand (COD), total organic carbon (TOC), aromaticity, H_2O_2 consumption and dissolved metal species, in order to optimize the operating parameters. Five-day biochemical oxygen demand (BOD_5) was determined in order to estimate the effect of CWPO on the biodegradability of the liquid effluent. Total heterotrophic bacteria were estimated in order to assess the effect of CWPO on the autochthonous microbial population of the liquid effluent. Additional microbiological assays were performed in order to evaluate the antimicrobial activity of the liquid effluent before and after treatment by CWPO.

2. Materials and methods

2.1. Chemicals

4-Nitrophenol, 4-NP ($O_2NC_6H_4OH$, Mr 139.11, 98 wt.%), hydrogen peroxide (H_2O_2, 30% w/v) and potassium phthalate monobasic (99.5 wt.%) were purchased from Acros Organics and Fluka and Riedel-de Haën, respectively. Iron (III) chloride hexahydrate ($FeCl_3.6H_2O$, 97 wt.%),

phenol (99.5 wt.%), formaldehyde solution (37 wt.%, stabilized with methanol), potassium dichromate (99.5 wt.%), mercury (II) sulphate ($HgSO_4$, 99 wt.%), ammonium hydroxide solution (25 wt.%) and silver nitrate (99.8 wt.%) were obtained from Panreac. Titanium (IV) oxysulphate ($TiOSO_4 \cdot xH_2O$, 15 wt.% in diluted sulphuric acid, 99.99%), iron (II) chloride tetrahydrate ($FeCl_2.4H_2O$, 99 wt.%), copolymer pluronic F127, ethanol absolute (99.8 wt.%) and sodium sulphite (Na_2SO_3, 98 wt.%) were purchased from Sigma-Aldrich. Nickel (II) chloride hexahydrate ($NiCl_2.6H_2O$, 95 wt.%), cobalt (II) chloride hexahydrate ($CoCl_2.6H_2O$, 99 wt.%), sodium hydroxide (NaOH, 98.7 wt.%), sulphuric acid (H_2SO_4, 95 wt.%), hydrochloric acid (HCl, 37 wt.%), silver sulphate (95 wt.%), methanol (HPLC grade), glacial acetic acid (analytical reagent grade), tert-butanol (99.8 wt.%), acetonitrile (HPLC grade) and potassium chromate (99.6 wt.%) were obtained from Fisher Chemical. Plate count agar (PCA), Muller Hinton agar (MHA) and nutrient broth (NB) were purchased from Liofilchem.

All chemicals were used as received, without further purification. Distilled water was used throughout the work.

2.2. Liquid effluent from a mechanical biological treatment plant for municipal solid waste

The liquid effluent used in this work was collected from a MBT plant for MSW located in Northern Portugal. The liquid effluent, whose properties are summarized in Table 1, gathers all the wastewater produced in the plant (mainly composed by a mechanical unit for residue sorting, followed by an anaerobic digestion unit for biogas production from the organic fraction of the MSW). The liquid effluent was filtered (analytical filter paper, 25 μm) prior to its use in this work, in order to remove the suspended solids that would interfere in subsequent treatment and analytical steps.

TABLE 1

2.3. Magnetic nanoparticles

Magnetite (Fe_3O_4) was synthesised by co-precipitation of Fe^{2+} and Fe^{3+} in basic solution, at 30 ºC and under N_2 atmosphere, as previously described [9]. For that purpose, 13.44 mmol of iron (II) chloride tetrahydrate and 26.88 mmol of iron (III) chloride hexahydrate were dissolved in 250 mL of distilled water and transferred into a 500 mL glass reactor, equipped with a condenser and immersed in an oil bath with controlled temperature. When the desired temperature was reached, the mixture was deaerated during 10 min with N_2 under vigorous stirring, and further kept under inert atmosphere. At this point, 10 mL of ammonium hydroxide solution (25 wt.%) was quickly added, a black precipitate being instantly obtained. Afterwards, possible residues of the precursors were washed-out with distilled water, the sample being then dried in an oven at 60 ºC for 24 h, resulting in the Fe_3O_4 material.

Cobalt ferrite ($CoFe_2O_4$) was synthesized by co-precipitation of Co^{2+} and Fe^{3+} in basic solution at 75 ºC, adapting the procedure described elsewhere [22]. For that purpose, 67 mmol of cobalt (II) chloride hexahydrate and 134 mmol of iron (III) chloride hexahydrate were dissolved in 100 mL of distilled water and transferred into a 250 mL glass reactor, equipped with a condenser and immersed in an oil bath with controlled temperature. When the desired temperature was reached, 80 mL of ammonium hydroxide solution (1 mol L^{-1}) was added dropwise using a peristaltic pump, under constant vigorous stirring. After the colour of the solution turned to dark-brown, the mixture was kept under vigorous stirring for an additional 30 min, in order to ensure the complete formation of ferrite crystals. Possible residues of the precursors were washed-out with distilled water and absolute ethanol, the sample being then dried in oven at 60 ºC for 24 h, ground into fine powder and treated under a purified air flow (100 cm^3 min^{-1}) at 500 ºC for 2 h with a heating ramp of 2 ºC min^{-1}, allowing crystallization of the materials with the inverse spinel structure [22, 23], and resulting in the $CoFe_2O_4$ sample. Nickel ferrite ($NiFe_2O_4$) was synthesized using the same procedure, except that the cobalt precursor was replaced by nickel (II) chloride hexahydrate.

2.4. Hybrid magnetic graphitic nanocomposites

The MGNC materials were prepared by hierarchical co-assembly of magnetic nanoparticles and carbon precursors, followed by thermal treatment, adapting the procedure previously described [9]. For that purpose, 5 g of copolymer pluronic F127 was dissolved in 50 mL of H_2O, in a round bottom 500 mL glass reactor equipped with a condenser and immersed in an oil bath with temperature control. Then, 5 mL of magnetic nanoparticles suspension (17 mg mL^{-1}, previously obtained by dispersion of Fe_3O_4, $NiFe_2O_4$ or $CoFe_2O_4$, in H_2O in an ultrasonic bath) was added, the resulting solution being stirred during 2 h at 66 ºC for homogenization. After that, ≈ 60 mL of a phenol/formaldehyde resol solution was added, the resulting mixture being kept under stirring (400 rpm) at 66 ºC for 72 h and then at 70 ºC for an additional 24 h. The phenol/formaldehyde resol solution was prepared by dissolution of 2.0 g of phenol in 7.0 mL of formaldehyde 37 wt.% solution, to which 50.0 mL of NaOH 0.1 mol L^{-1} was added, the solution being then kept under stirring at 70 ºC for 30 min.

In each case, the recovered solids were washed with distilled water in order to promote the washing-out of some possible residues of the precursors and then dried overnight in oven at 60 ºC. Afterwards, each sample was thermally treated under a N_2 flow (100 cm^3 min^{-1}) at 120, 400 and 600 ºC during 60 min at each temperature and then at 800 ºC for 240 min, defining a heating ramp of 2 ºC min^{-1}. Finally, each sample was washed with 1 L of distilled water at 50 ºC under vacuum filtration, and then with 1 L of HCl solution (pH = 3), also at 50 ºC under vacuum filtration, being then dried overnight in oven at 60 ºC, resulting in the Fe_3O_4/MGNC, $NiFe_2O_4$/MGNC or $CoFe_2O_4$/MGNC materials.

2.5. Characterization techniques

X-ray diffraction (XRD) analysis was performed in a PANalytical X'Pert MPD equipped with a X'Celerator detector and secondary monochromator (Cu Kα λ = 0.154 nm; data recorded at a 0.017º step size). The crystallographic phases present were identified using

HighScore software and Crystallography Open Database. Rietveld refinement of the XRD diffraction patterns was performed using PowderCell software allowing phase quantification. Crystallite sizes were determined by the Williamson-Hall method.

Transmission electron microscopy (TEM) was performed in a LEO 906E instrument operating at 120 kV, equipped with a 4 Mpixel 28 × 28 mm CCD camera from TRS. At least 100 counts were performed by using ImageJ software in order to estimate the size of the magnetic nanoparticles. At least 65 counts were performed to estimate the size of the metal core of the MGNC materials.

The textural properties were determined from N_2 adsorption–desorption isotherms at -196 ºC, obtained in a Quantachrome NOVA 4200e adsorption analyser, as previously described [24]. The pH at point of zero charge (pH_{PZC}) was obtained by pH drift tests [24]. Thermogravimetric analysis (TGA) was performed using a Netzsch TG 209 F3 Tarsus equipment under oxidative atmosphere, upon heating the samples from 30 to 950 ºC at 20 ºC min^{-1}.

2.6. Catalytic wet peroxide oxidation experiments

Batch CWPO experiments with 4-NP as model pollutant were performed in a well-stirred (600 rpm) glass reactor equipped with a condenser, a temperature measurement thermocouple, a pH measurement electrode and a sample collection port. The reactor was loaded with 4-NP aqueous solutions (5.0 g L^{-1}) and heated by immersion in an oil bath at controlled temperature. Upon stabilization at 80 ºC, the solution pH was adjusted to 3 by means of H_2SO_4 and NaOH solutions, and the experiments were allowed to proceed freely, without further pH conditioning. A calculated volume of H_2O_2 (30% w/v) was injected into the system, in order to reach the stoichiometric amount of H_2O_2 needed to completely mineralise 4-NP (17.8 g L^{-1}). The catalyst was added after complete homogenization of the resulting solution, that moment being considered as t_0 = 0 min. Pure adsorption runs were also performed in order to assess the

possible adsorption influence on the 4-NP removal by CWPO, but, in this case, the amount of H_2O_2 was replaced by distilled water. Blank experiments, without any catalyst, were also carried out to assess possible non-catalytic oxidation promoted by H_2O_2.

In order to show the predominant role of heterogeneous catalysis promoted by $CoFe_2O_4$/MGNC, a leaching test was performed as previously described [9]. For that purpose, the $CoFe_2O_4$/MGNC catalyst was removed after 30 min of reaction at the reaction temperature (80 ºC), and the reaction solution was allowed to progress further. The participation of the $HO^{\bullet}$ radicals in the CWPO process was indirectly shown by adding tert-butanol (tBuOH) – a strong $HO^{\bullet}$ scavenger [25].

Batch CWPO experiments with the liquid effluent described in Section 2.2 were performed under the same experimental conditions described for the CWPO runs performed with 4-NP solutions, except that the concentration of H_2O_2 was in the range 13.9 – 34.7 g L^{-1} (corresponding to 0.6 and 1.6-fold the stoichiometric amount theoretically needed to reduce the effluent COD and to react with the effluent chlorides), and the operating pH in the range 2.5 – 8.

The in-situ magnetic separation of the catalyst was performed after the reaction stage, by coupling a Mitutoyo 7033B switchable magnetic stand (clamping force 600 N) with the glass reactor used for CWPO. Briefly, the magnetic stand is composed by four parts: a non-ferrous metal spacer placed between two plates or iron, and the magnet at the centre; when the magnet poles are aligned with the ferrous plates the magnetic stand is ON, whereas the magnetic stand is OFF when the magnet poles are aligned with the non-ferrous spacer. When the round bottom glass reactor was placed on the magnetic stand, it was immediately switched ON and the magnetic separation was allowed to proceed during 5 min. Afterwards, the treated water was collected with a pipette. In order to evaluate the stability of the $CoFe_2O_4$/MGNC catalyst in the CWPO of the liquid effluent from the MBT plant, reusability cycles were performed as described: after each run, in-situ magnetic separation was employed for catalyst recovery and

the treated water was collected. Afterwards, 23 wt.% of the initial catalyst load was added (i.e., 0.115 g L^{-1}; corresponding to the mass fraction lost due to the sampling procedure and to the treated water collection) in order to ensure equal catalyst dosage throughout all the reusability cycles (0.5 g L^{-1}), and the catalyst was reused in CWPO upon the addition of fresh liquid effluent.

Selected experiments were performed in duplicate, in order to assess reproducibility and error of the experimental results. It was found that the standard deviation of the 4-NP and H_2O_2 determinations was never superior to 1% in the experiments performed with the model pollutant, while in the experiments performed with the liquid effluent from a MBT plant, the standard deviation of the COD, TOC, H_2O_2 and aromaticity determinations was never superior to 2%, 1%, 4% and 1%, respectively.

2.7. Analytical methods

The parent compound 4-NP and possible oxidation by-products were determined by high performance liquid chromatography (HPLC), using a method previously described [26]. Total organic carbon (TOC) was determined using a Shimadzu TOC-L CSN analyser. For quantification purposes, small aliquots were periodically withdrawn from the reactor and an excess of sodium sulphite was immediately added in order to consume residual H_2O_2 and to instantaneously stop the reaction.

The concentration of H_2O_2 was followed by a colorimetric method with titanium (IV) oxysulfate [26]. Chemical oxygen demand (COD) was determined by a closed reflux colorimetric method, adapting the procedure described elsewhere [27]. A 10:1 weight ratio of $HgSO_4$:Cl^- was ensured in all the analysis in order to avoid the interference of chloride ion [27]. The apparent COD value obtained (COD_{app}) was then corrected considering the theoretical interference of residual H_2O_2, as described in Eq. 1, which was given elsewhere [28], and confirmed in the present study (considering the concentration range $0 \leq [H_2O_2] \leq 692$ mg L^{-1}).

Absorbance spectra in the range 200 – 660 nm were obtained with a 0.5 nm sampling interval, using a T70 spectrometer (PG Instruments, Ltd.). Aromaticity was estimated by measuring the absorbance at 254 nm – a wavelength at which most aromatic compounds typically present a maximum value of absorbance [29]. The contribution of residual H_2O_2 on aromaticity was experimentally determined using H_2O_2 standard solutions in the range 10 – 14,000 mg L^{-1}. Afterwards, the apparent aromaticity value obtained ($Aromaticity_{app}$) was corrected considering the interference of residual H_2O_2, as described in Eq. 2.

The five-day biochemical oxygen demand (BOD_5) was determined by the standardised respirometric OxiTop® method (WTW, Weilheim, Germany). For that purpose, an appropriate volume of sample was added into a brown glass bottle (nominal volume 510 mL) equipped with a magnetic stirrer and a carbon dioxide trap in the headspace (NaOH pellets). Each bottle was sealed with an OxiTop® head and then placed in an incubator box at constant temperature (20 ^oC) during the five-day incubation period. The BOD_5 value was calculated from the pressure decrease in the closed vessel, as recorded via the piezoresistive electronic pressure sensors of the OxiTop® measuring system. In the samples collected after CWPO, the apparent BOD_5 value obtained ($BOD_{5,\ app}$) was then corrected considering the theoretical interference of residual H_2O_2, as described in Eq. 3.

The samples collected for the determination of H_2O_2, COD, absorbance spectra, aromaticity and BOD_5 were immediately placed in ice in order to stop the reaction, and kept at 3 ^oC until the analysis. Appropriate dilutions were made when necessary.

$$COD = COD_{app} - 0.4706\ [H_2O_2] / \text{mg L}^{-1} \quad \textbf{(1)}$$

$$Aromaticity = Aromaticity_{app} - 0.0005\ [H_2O_2]] / \text{mg L}^{-1} \quad \textbf{(2)}$$

$$BOD_5 = BOD_{5,\ app} + 0.4706\ [H_2O_2] / \text{mg L}^{-1} \quad \textbf{(3)}$$

Total Fe content was determined by a colorimetric method with 1,10-phenantroline, according to ISO 6332 and measuring the absorbance at 510 nm [30]. The same analytical

procedure was employed for the determination of the dissolved Fe content, except that in this case the samples were filtered (0.2 μm) prior to the analysis. Likewise, dissolved Ni and Co contents were determined by using a PerkinElmer PinAAcle 900 atomic absorption spectrometer, employing a multi-element hollow cathode lamp (Lumina N3050214). The concentration of chlorides dissolved in the liquid effluent was determined by the Mohr method (titration with silver nitrate, using potassium chromate as indicator).

2.8. Microbiological assays

Heterotrophic plate count by the spread plate method was used in order to estimate the number of live heterotrophic bacteria in the liquid effluent before and after treatment by CWPO [31]. For that purpose, 0.1 mL of starting sample and serial 10-fold dilutions were spread onto PCA plates under aseptic conditions and incubated at 28 ºC during 5 days; counting was performed for plates displaying 10 – 100 colony-forming units (CFU), the results being reported as CFU per millilitre (CFU mL^{-1}). All the procedure was performed in triplicate.

The agar disk-diffusion method was used for the antimicrobial susceptibility testing of the liquid effluent before and after treatment by CWPO [32]. *Klebsiella pneumoniae* (Gram negative) and *Bacillus cereus* (Gram positive) were selected as test microorganisms. In each case, the bacteria were initially grown overnight in NB at 37 ºC. Afterwards, MHA plates were inoculated with standardized inocula of the test microorganisms (0.5 McFarland; corresponding to 10^8 CFU mL^{-1}). Then, antibiotics testing paper discs (6 mm diameter; Filtres Fioroni) containing 10 μL of the testing solution, previously sterilized by filtration (0.2 μm), were placed on the agar surface. Finally, possible inhibition growth zones surrounding the paper discs were evaluated after 16 and 24 h of incubation at 37 ºC. The whole procedure was performed in triplicate.

3. Results and discussion

3.1. Materials characterization

Both the magnetic nanoparticles and the resulting MGNC materials developed for this work were extensively characterized. XRD and TEM analysis were performed in order to assess the molecular structure and morphology of these materials, the corresponding results being given in Figures 1 and 2, respectively. Fe_3O_4 exhibits the typical diffraction pattern of magnetite, with a lattice parameter a = 8.357 Å and a crystallite size of 16.6 ± 0.2 nm (cf. Figure 1a). As observed in Figure 1b, an impure phase was found in the diffraction pattern of $NiFe_2O_4$ in addition to nickel ferrite (a = 8.330 Å, crystallite size of 10.2 ± 0.5 nm), which was ascribed to the thermal treatment required for the crystallization of the amorphous materials with the inverse spinel structure. This additional phase was identified as hematite (a = 5.015 Å, c = 13.75 Å, crystallite size of 16.6 ± 1.0 nm), corresponding to 21 wt.% of $NiFe_2O_4$, as determined by XRD analysis. As observed in Figure 1c, a similar phenomenon occurred during the synthesis of $CoFe_2O_4$. In this case hematite (a = 5.043 Å, c = 13.78 Å, crystallite size of 24.2 ± 0.5 nm) was found in addition to cobalt ferrite (a = 8.387 Å, crystallite size of 14.3 ± 0.2 nm), the impure phase corresponding to 24 wt.% of $CoFe_2O_4$.

As detailed in our previous work [9], Fe_3O_4 nanoparticles were successfully encapsulated within a graphitic structure during the synthesis of Fe_3O_4/MGNC, resulting in a core-shell structure (cf. Figure 2a). As observed in Figure 1a, some changes in the magnetite phase occurred, maghemite (a = 8.379 Å), iron (a = 2.868 Å) and traces of hematite (proto) being identified in the diffraction pattern of Fe_3O_4/MGNC, in addition to magnetite (a = 8.343 Å) and graphite. Since magnetite nanoparticles are very sensitive to oxidation in the presence of oxygen, these phase modifications can be ascribed to the progressive oxidation of Fe^{2+} ions in the inverse spinel structure of magnetite to Fe^{3+} – most likely during the Fe_3O_4/MGNC

synthesis step performed in liquid phase (i.e., in oxidative media), resulting in its partial oxidation to maghemite and hematite [33, 34].

During the hierarchical co-assembly mechanism in the Fe_3O_4/MGNC synthesis, Fe_3O_4 nanocrystals grow and spontaneously co-assemble by partially replacing F127/resol micelles; at the same time, carbon-carbon bonds are formed with the polymerization of resols and, upon thermal treatment, the copolymer F127 is eliminated, graphitic carbon frameworks being obtained with the participation of Fe_3O_4 as graphitization catalyst [35]. The average size of the magnetic core of Fe_3O_4/MGNC, 109 ± 35 nm, as determined from TEM measurements (cf. Figure 2b), suggests that the cores are mainly composed by agglomerates of magnetic nanoparticles (with crystallite sizes in the range 23 – 165 nm, depending on the phase, as determined by XRD analysis). These observations are in accordance with the hierarchical co-assembly mechanism of the Fe_3O_4/MGNC synthesis.

$NiFe_2O_4$/MGNC and $CoFe_2O_4$/MGNC were prepared by the same procedure used for the synthesis of Fe_3O_4/MGNC, except that Fe_3O_4 was replaced by $NiFe_2O_4$ and $CoFe_2O_4$, respectively. Therefore, the encapsulation of these magnetic nanoparticles within a graphitic shell is expected to occur through a similar route to that reported for Fe_3O_4. As observed in Figures 2c and e, both $NiFe_2O_4$ and $CoFe_2O_4$ nanoparticles were successfully encapsulated within graphitic structures during the synthesis of $NiFe_2O_4$/MGNC and $CoFe_2O_4$/MGNC, respectively, resulting in core-shell structures. Regarding the molecular structure, nickel (a = 3.575 Å, crystallite size of 33 ± 5 nm) was identified in the diffraction pattern of $NiFe_2O_4$/MGNC, in addition to nickel ferrite (a = 8.348 Å, crystallite size of 19 ± 3 nm) and graphite (cf. Figure 1b); iron (a = 2.858 Å, crystallite size of 44 ± 1 nm) was identified in the diffraction pattern of $CoFe_2O_4$/MGNC, in addition to cobalt ferrite (a = 8.363 Å, crystallite size of 33 ± 2 nm) and graphite (cf. Figure 1c). Once again, when the average size of the magnetic cores of $NiFe_2O_4$/MGNC and $CoFe_2O_4$/MGNC (36 ± 15 nm and 56 ± 18 nm respectively, as determined from TEM measurements, cf. Figures 2d and f), are compared to the size of parent

$NiFe_2O_4$ and $CoFe_2O_4$ (11 ± 3 nm and 14 ± 4 nm respectively, cf. the insets of Figures 2d and f), it is suggested that the cores of these MGNC materials are mainly composed by agglomerates of magnetic nanoparticles.

FIGURE 1

FIGURE 2

The texture and surface chemistry of the MGNC materials were further characterized by TGA analysis, N_2 adsorption-desorption isotherms and pH_{PZC}. The TGA analysis of Fe_3O_4/MGNC (cf. Figure S1a, in supplementary material) reveals 27.3 wt.% of ashes, corresponding to the mass fraction of Fe_3O_4 encapsulated in Fe_3O_4/MGNC. Likewise, the ash contents of $NiFe_2O_4$/MGNC and $CoFe_2O_4$/MGNC are 10.4 wt.% and 14.4 wt.%, respectively (cf. Figure S1b and c). It was also found that all the MGNC materials are stable up to 400 ºC under oxidizing atmosphere. The N_2 adsorption-desorption isotherms at -196 ºC of the MGNC materials (cf. Figure S2) denote the presence of mesoporosity (as revealed by the progressive increase of the amount of N_2 adsorbed at higher relative pressures) and microporosity (as revealed by the amount of N_2 adsorbed at low relative pressure). The detailed textural properties of the MGNC materials are given in Table 2. As observed, similar textural properties are obtained regardless of the composition of the magnetic core. Nevertheless, as reflected by the pH_{PZC} values also given in Table 2, the overall surface chemistry is slightly affected. If the values of pH_{PZC} obtained for Fe_3O_4/MGNC (7.1), $NiFe_2O_4$/MGNC (8.7) and $CoFe_2O_4$/MGNC (9.0) are compared with those recently reported in the literature for their main metal oxide constituents [36, 37], namely Fe_3O_4 (6.2 – 7.4), $NiFe_2O_4$ (6.7 – 10.2) and $CoFe_2O_4$ (7.5 – 10.1), it is suggested that the pH_{PZC} of the MGNC materials are mainly determined by the different contributions of the metal oxides detected by XRD.

TABLE 2

3.2. Screening of the hybrid magnetic graphitic nanocomposites in CWPO

The performance of the MGNC materials when applied in CWPO was initially evaluated through experiments performed with highly loaded 4-NP solutions (5 g L^{-1}, corresponding to a TOC content similar to that of the liquid effluent considered in Section 3.4), under the experimental conditions described in Section 2.6. In order to optimize the efficiency of catalyst usage, the catalyst dosage was kept very low when compared to the pollutant concentration, with a fixed pollutant/catalyst mass ratio as high as 10. As observed in Figure 3, the 4-NP removal obtained after 8 h in the non-catalytic experiment is negligible when compared to that obtained in the presence of the MGNC catalysts. Among the composite materials, the catalyst resulting from the inclusion of $CoFe_2O_4$ within a carbon shell ($CoFe_2O_4$/MGNC) reveals the highest activity for the CWPO of 4-NP. In this case, complete 4-NP conversion is obtained in 3 h, corresponding to a very high pollutant mass removal of 3333 mg g^{-1} h^{-1}. This enhanced activity in CWPO can be ascribed to the presence of Co species, as observed in previous works [24, 38]. The apparent catalytic activity of the material resulting from the inclusion of $NiFe_2O_4$ within a carbon shell ($NiFe_2O_4$/MGNC) is also superior to that obtained with the material with the Fe_3O_4 core (Fe_3O_4/MGNC). However, by comparing the leaching of Fe species at the end of the CWPO runs performed with Fe_3O_4/MGNC (1.8 mg L^{-1}), $NiFe_2O_4$/MGNC (3.2 mg L^{-1}) and $CoFe_2O_4$/MGNC (0.9 mg L^{-1}), it is observed that the $NiFe_2O_4$/MGNC catalyst exhibits the lowest stability. On the contrary, the $CoFe_2O_4$/MGNC catalyst reveals an enhanced resistance to the leaching of Fe species, which can also be ascribed to the presence of Co species, as detailed in a previous work [38]. However, as Co is oxidized during CWPO, its susceptibility to undergo leaching to the treated waters is expected to increase [38]. In order to confirm this hypothesis, the leaching of Co from the $CoFe_2O_4$/MGNC catalyst was determined at the end of the CWPO run depicted in Figure 3. Although under these conditions the leaching of Co amounts to 10.7 mg L^{-1}, there are a lack of standards for treated wastewater and even for

drinking water [39]. Likewise, the leaching of Ni species at the end of the CWPO experiment performed with $NiFe_2O_4$/MGNC was also determined (4.2 mg L^{-1}).

FIGURE 3

Due to the best overall performance in the screening experiments, $CoFe_2O_4$/MGNC was object of additional studies. A pure adsorption run was performed in order to assess the possible adsorption influence on the removal of 4-NP by CWPO. As observed in Figure 4a, the removal of 4-NP obtained in the pure adsorption run performed with $CoFe_2O_4$/MGNC is negligible, corresponding to 0.7% of the initial content of 4-NP. This negligible percent adsorption removal of 4-NP can be ascribed to the very low $CoFe_2O_4$/MGNC dosage when compared to the pollutant concentration, as reflected by the 4-NP/catalyst mass ratio of 10. The evolution of COD, TOC and H_2O_2 consumption during the CWPO run performed with $CoFe_2O_4$/MGNC is also shown in Figure 4a. As observed, TOC and COD removals of 54.4% and 74.2% were respectively obtained. At the same time, the consumption of H_2O_2 amounts to 71.0%, representing high efficiencies of TOC and COD removals per unit of H_2O_2 decomposed.

A leaching test was performed in order to evaluate the heterogeneous nature of the $CoFe_2O_4$/MGNC catalyst, as described in Section 2.6. As observed in Figure 4b, when the $CoFe_2O_4$/MGNC catalyst is removed after 30 min of reaction, the reaction solution reveals negligible activity in the CWPO of 4-NP, considering both 4-NP and TOC removals. This observation confirms the predominant role of heterogeneous CWPO promoted by $CoFe_2O_4$/MGNC.

The participation of $HO^{\bullet}$ radicals in the process was indirectly evaluated. For that purpose, tert-butanol (tBuOH) – a strong $HO^{\bullet}$ scavenger [25], was added before a CWPO experiment performed in the presence of $CoFe_2O_4$/MGNC. When the CWPO runs performed in the presence and absence of tBuOH are compared (cf. Figure 4c), it is observed that the removal of 4-NP is greatly suppressed by tBuOH. Although not directly supported by quantification of the $HO^{\bullet}$ radicals formed during the process, this indirect result suggests the ability of

$CoFe_2O_4$/MGNC to efficiently promote the decomposition of H_2O_2 via HO• formation. Furthermore, the aromatic by-products detected during the CWPO of 4-NP in the presence of $CoFe_2O_4$/MGNC (cf. Figure 5a) are in agreement with a reaction mechanism including the attack of the 4-NP molecule by HO• radicals, as reported in our previous works [9, 26]. Further attack of HO• radicals on the aromatic intermediate compounds leads to the opening of the aromatic ring, and thus to the formation of a series of low molecular weight carboxylic acids (cf. Figure 5b). In addition, NO_3^- can be produced from the $–NO_2$ group subtraction from the 4-NP aromatic ring under the oxidation conditions employed [26]. Based on the NO_3^- concentrations shown in Figure 5b, it can be concluded that at least 50.8% of the total nitrogen initially present in the 4-NP 5 g L^{-1} solution was effectively subtracted from the main aromatic ring after 4 h of CWPO in the presence of the $CoFe_2O_4$/MGNC catalyst.

FIGURE 4

FIGURE 5

3.3. Development of an in-situ magnetic separation system for catalyst recovery

In order to take advantage of the magnetic properties of $CoFe_2O_4$/MGNC, a lab-scale magnetic separation system was designed for in-situ catalyst recovery after the CWPO reaction stage. For that purpose, a switchable magnetic stand was coupled with the reactor after the reaction stage (as described in Section 2.6.), allowing to perform reaction/separation sequential stages in a single vessel, thus avoiding the separation of the heterogeneous catalysts by filtration and/or centrifugation. As observed in Figure 6, this technique was successfully employed for the recovery of the $CoFe_2O_4$/MGNC catalyst after the CWPO run performed with 4-NP (5 g L^{-1}), ca. 98% of the treated water being collected. An image of the glass reactor coupled with the magnetic stand is provided in Figure 6a. In order to estimate the efficiency of catalyst recovery, the $CoFe_2O_4$/MGNC collected after the CWPO run was dried overnight at 60 ºC and then weighed. Reaction/separation sequential experiments performed in triplicate allowed to

determine the percentage of catalyst recovery. It was found that 77.0 ± 6.1 wt.% of the initial $CoFe_2O_4$/MGNC load is recovered by implementing the proposed in-situ magnetic separation system, a value well above the 57.9 ± 2.4 wt.% recovered by conventional filtration. The direct benefit of magnetic separation for the recovery of the catalyst in the same unit that is used in the CWPO experiments is thus demonstrated. With this in mind, in-situ magnetic separation will be further explored in the reusability cycles performed in Section 3.4.3.

FIGURE 6

3.4. CWPO of the liquid effluent from a MBT plant for municipal solid waste

Herein, the suitability of the most active and stable catalytic system obtained in Section 3.2 for the CWPO of the liquid effluent collected from a MBT plant is evaluated. As detailed in Table 1, this effluent contains a high pollutant load, due to the presence of organic (9,206 mg L^{-1} COD; 2,046 mg L^{-1} TOC), inorganic (14,350 mg L^{-1} bicarbonates; 2,833 mg L^{-1} chlorides) and biological (14.7×10^4 CFU mL^{-1} total heterotrophic bacteria cultivable at 28 ºC) species. According to the BOD_5/COD ratio, which is widely used as an indicator of the biodegradability of liquid effluents, a wastewater is considered easily treatable by biological means if the BOD_5/COD ratio is 0.5 or larger [31]. On the contrary, a BOD_5/COD ratio below 0.3 suggests the presence of toxic components, the wastewater being not biodegradable or acclimated microorganisms being required for its biological treatment [31]. The liquid effluent considered in this work is not expected to be prone to degradation by conventional biological treatments, according to the low BOD_5/COD ratio of 0.21. It is also known that both bicarbonates and chlorides can act as $HO^{\bullet}$ radical scavengers. Although several reactions involving bicarbonate and chloride ions may occur in the bulk, the $HO^{\bullet}$ radical scavenging effect promoted by these inorganic species results mainly from their direct reaction with $HO^{\bullet}$ radicals. The reaction of bicarbonate ions with $HO^{\bullet}$ radicals can be described by Eq. 4 [40], while the reaction of chloride ions with $HO^{\bullet}$ radicals proceeds through the mechanism described by Eqs. 5 and 6 [41].

Therefore, the presence of these inorganic species is expected to hinder the performance of CWPO for the treatment of the liquid effluent considered in this work. Bearing this in mind, the operating conditions that maximize the performance of CWPO for the treatment of the liquid effluent from the MBT plant in the presence of $CoFe_2O_4$/MGNC were thoroughly investigated.

$$HO^{\bullet} + HCO_3^- \rightarrow CO_3^{\bullet-} + H_2O \quad \textbf{(4)}$$

$$HO^{\bullet} + Cl^- \rightarrow HOCl^{\bullet-} \quad \textbf{(5)}$$

$$HOCl^{\bullet-} + H^+ \rightarrow Cl^{\bullet} + H_2O \quad \textbf{(6)}$$

3.4.1. CWPO process optimization: the crucial role of the operating pH

The operating conditions used in Section 3.2 were initially employed in this Section, the catalyst dosage being kept very low when compared to the effluent COD. Taking into account the possible catalytic contribution of the Fe species present in the liquid effluent collected from the MBT plant (6.4 mg L^{-1}, cf. Table 1), a preliminary experiment was performed without added catalyst. In spite of the Fe content and the high complexity of the liquid effluent, the COD removal obtained after 24 h of reaction under these conditions was only 12.8%, representing less than a third of that obtained in the presence of $CoFe_2O_4$/MGNC (0.5 g L^{-1}). This result highlights the role of CWPO promoted by $CoFe_2O_4$/MGNC.

Seeking for CWPO process optimization, the influence of H_2O_2 dosage was then evaluated. Based on the results obtained in CWPO runs performed with H_2O_2 concentrations in the range 13.9 – 34.7 g L^{-1} (results not shown), it was found that the best performance is achieved when employing $[H_2O_2]_0$ = 27.7 g L^{-1} (corresponding to 1.2-fold the stoichiometric amount theoretically needed to reduce the effluent COD and to neutralize the $HO^{\bullet}$ radical scavenging effect promoted by the chlorides dissolved in the effluent, as described by Eqs. 5 and 6). Therefore, additional experiments were performed with this H_2O_2 dosage.

It is noteworthy that the bicarbonate equilibrium concentration in water depends on the pH, as described by the acid ionization reactions, Eqs. 7-8, and corresponding acid-dissociation

constants [42]. At the natural pH of the liquid effluent considered in this work (8.2) and given concentrations of dissolved matter and ions, the prevailing species is the bicarbonate ion (HCO_3^-). In addition to the $HO^\bullet$ radical scavenging described by Eq. 4, the negative effect of HCO_3^- is particularly significant in the case of CWPO, since H_2O_2 can be directly decomposed through the parasitic reaction described by Eq. 9 [43], even before $HO^\bullet$ formation. However, this parasitic reaction can be avoided by decreasing the solution pH to values below 6.35; in this case, HCO_3^- is converted to carbonic acid (H_2CO_3) – which is subsequently decomposed into carbon dioxide (which escapes the solution for the gas phase) and water (cf. Eq. 10) [44]. Therefore, based on the presence of bicarbonate species (14,350 mg L^{-1}), operating at pH < 6.35 is expected to favour the performance of CWPO for the treatment of the liquid effluent considered in this work.

$$H_2CO_3(aq) \leftrightarrows H^+(aq) + HCO_3^-(aq) \qquad pK_{a1} = 6.35 \qquad \textbf{(7)}$$

$$HCO_3^-(aq) \leftrightarrows H^+ + CO_3^{2-}(aq) \qquad pK_{a2} = 10.33 \qquad \textbf{(8)}$$

$$HCO_3^-(aq) + H_2O_2(aq) \leftrightarrows HCO_4^-(aq) + H_2O(aq) \qquad \textbf{(9)}$$

$$H_2CO_3(aq) \leftrightarrows CO_2(g) + H_2O(l) \qquad \textbf{(10)}$$

Nevertheless, the presence of chlorides should also be taken into account in this analysis. As discussed elsewhere for the H_2O_2/UV process, the solution pH can also affect the extent of the $HO^\bullet$ radical scavenging reaction described by Eq. 5 [45]. Specifically, the rate constant for the reaction described in Eq. 5 is 4.3×10^9 L mol^{-1} s^{-1}; however, the hypochlorous radical ($HOCl^{\bullet-}$) formed by the reaction described in Eq. 5 is able to dissociate back to $HO^\bullet$ radical and chloride ion (Cl^-), the dissociation rate constant being 6.1×10^9 s^{-1} [45]. As described by Eq. 6, $HOCl^{\bullet-}$ can also be converted into chlorine radicals ($Cl^\bullet$) and water through a protonation reaction with the rate constant of 2.1×10^{10} L mol^{-1} s^{-1}, in this case the reverse rate reaction being much smaller (1.3×10^3 s^{-1}) [45]. Therefore, it is expected that the formation of $Cl^\bullet$ by the protonation

reaction described in Eq. 6 increases as the solution pH decreases, thus promoting the scavenging reaction described by Eq. 5. In this case, the critical point affecting the extent of $HO^{\bullet}$ radical scavenging is the p*K*a of the reverse reaction (i.e., the deprotonation reaction) described by Eq. 6 (7.2). Thus, it can be concluded that $Cl^{\bullet}$ is the prevailing species at solution pH < 7.2, while $HOCl^{\bullet-}$ becomes the dominant species when pH > 7.2, thus decreasing the consumption of $HO^{\bullet}$ radicals by the reaction described by Eq. 5. Therefore, based on the presence of chloride species (2,833 mg L^{-1}), operating pH > 7.2 is expected to favour the performance of CWPO for the treatment of the liquid effluent considered in this work.

Summarizing, the solution pH is expected to significantly affect the performance of CWPO for the treatment of the effluent from the MBT plant. On one hand, pH < 6.35 limits the negative effect of bicarbonates; while, on the other hand, pH > 7.2 limits the negative effect of chlorides. Therefore, the selection of the optimum pH may be considered as the crucial step to achieve the operating parameters that maximize the performance of the liquid effluent treatment by CWPO in the presence of $CoFe_2O_4$/MGNC.

Bearing this in mind, the individual effect of the operating pH on the efficiency of CWPO was evaluated in the range 2.5 – 8. For that purpose, COD, TOC, aromaticity and H_2O_2 conversions were determined, as shown in Figure 7a. The efficiency of CWPO for the treatment of the liquid effluent from the MBT plant tends to increase as the pH increases in the range 2.5 – 6, whereas it dramatically decreases for pH > 6. This phenomenon – which can be ascribed to the presence of bicarbonates and chlorides – confirms the crucial role of the operating pH in the CWPO of the liquid effluent considered in this work, as previously discussed. At pH > 6, 97% of the initial H_2O_2 dosage is consumed within the first 30 min of reaction, most likely due to the fast reaction with HCO_3^-, as described by Eq. 9. At pH < 6, the $HO^{\bullet}$ radical scavenging by Cl^- is increasingly significant, thus hindering the efficiency of the CWPO process. Therefore, pH = 6 can be considered the optimum operating pH, since it allows to maximize the performance of the liquid effluent treatment by CWPO in the presence of $CoFe_2O_4$/MGNC.

Additional insights on the COD, TOC, H_2O_2 and aromaticity conversions, and absorbance spectra evolution as a function of time in the CWPO run performed under the optimized conditions are given in Figures 7b and c, respectively. As observed, fast conversions of COD, TOC, aromaticity and H_2O_2 are obtained in the first 8 h of CWPO. Up to that point, ca. 93% of the effluent aromaticity is already converted; while from 8 to 24 h of reaction, an increase of only ca. 2% is observed in the aromaticity conversion. However, the TOC content of the effluent decreases ca. 14% during the same period, while the absorbance spectra also evolved favourably (cf. Figure 7c), revealing that the treatment reactions still proceed although at a lower rate. These observations suggest that recalcitrant by-products are formed when the aromatic compounds are attacked by HO• radicals (cf. demonstrated in Section 3.2.). This mechanism is also suggested by the changes in the solution pH observed during the treatment by CWPO (cf. Figure 7b). Specifically, pH decreases from 6 (i.e., the initial pH) to 5.4 in the first 2 h, suggesting the formation of low molecular weight carboxylic acids; afterwards the pH gradually increases up to 6.5 at the end of the reaction, suggesting that the CWPO treatment is able to mineralize most of these carboxylic acids although at an apparently lower rate when broad parameters, like COD and TOC are considered. After 24 h of CWPO, ca. 95% of the effluent aromaticity is converted under these operating conditions, while ca. 55% of the initial COD and TOC are effectively removed. The H_2O_2 consumption during the treatment represents ca. 98% of the initial dosage.

The BOD_5 of the treated water was also determined in order to estimate the effect of CWPO on the biodegradability of the liquid effluent. It was found that the BOD_5 is slightly affected during the process, a decrease from 1,933 mg L^{-1} to 1,760 mg L^{-1} being observed. At the same time the COD decreased from 9,206 mg L^{-1} to 4,164 mg L^{-1}. Accordingly, the BOD_5/COD ratio of the treated water is 0.42, representing a 2-fold increase when compared to the BOD_5/COD ratio of the liquid effluent (0.21). A BOD_5/COD ratio in the range 0.3 – 0.5 suggests that the wastewater is treatable by biological means [31]. It can be therefore concluded that the

biodegradability of the liquid effluent is enhanced during the treatment by CWPO in the presence of $CoFe_2O_4$/MGNC.

In addition, the dissolved Fe content was measured at the end of the CWPO runs performed with operating pH in the range 2.5 – 6. The highest value was found in the experiment performed at pH = 2.5, corresponding to a Fe concentration of 1.04 mg L^{-1}; on the other hand, the lowest value was obtained in the experiment performed at pH = 6 (0.27 mg L^{-1}). However, it should be noted that the liquid effluent considered in this work is very complex. Although the total Fe content present in the effluent is 6.4 mg L^{-1}, the amount of dissolved Fe species, i.e., those obtained after filtration (0.2 μm), actually depends on the pH. For instance, the inherent dissolved Fe content of the effluent is 0.96 mg L^{-1} after 24 h at pH = 3, but this value decreases to 0.15 mg L^{-1} after 24 h at pH = 6. Therefore, the dissolved Fe content determined at the end of the CWPO runs cannot be fully ascribed to leaching from the $CoFe_2O_4$/MGNC catalyst. Likewise, the dissolved Co content at the end of the CWPO run performed at pH = 6 was also determined (0.58 mg L^{-1}); it can be considered very low, in particular when compared to the inherently dissolved Co content in the effluent (0.12 mg L^{-1}, cf. Table 1).

FIGURE 7

3.4.2. Disinfection and antimicrobial activity

Regarding the bacterial population, heterotrophic plate count is a procedure widely used to evaluate the performance of treatment processes, since it allows to estimate the number of live heterotrophic bacteria in a given water or wastewater [31]. As described in Section 2.8., the spread plate method was used in this work. The selected incubation temperature was 28 ºC, since it favours the growth of waterborne bacteria, thus yielding higher bacterial plate counts when compared to that obtained at lower or higher incubation temperatures [46-48]. Under this context, total heterotrophic bacteria in the treated water were estimated in order to assess the effect of CWPO on the effluent autochthonous microbial population (14.7×10^4 CFU mL^{-1} total

heterotrophic bacteria cultivable at 28 ºC). After incubation at 28 ºC during 5 days, not a single colony was found in the plate count performed in triplicate, even in the undiluted treated water samples. Therefore, although this was not the main goal of the treatment proposed, it can be concluded that disinfection of the effluent was achieved upon the CWPO treatment employed in the presence of $CoFe_2O_4$/MGNC under the optimum operating conditions considered (i.e., [$CoFe_2O_4$/MGNC] = 0.5 g L^{-1}, T = 80 ºC, pH = 6 and $[H_2O_2]_0$ = 27.7 g L^{-1}).

Additional microbiological assays were performed in order to evaluate the antimicrobial activity of the liquid effluent before and after treatment by CWPO. As described in Section 2.8., the agar disk-diffusion method was used for the antimicrobial susceptibility testing. For that purpose, *Klebsiella pneumoniae* (Gram negative) and *Bacillus cereus* (Gram positive) were selected as test microorganisms. After 16 and 24 h of incubation at 37 ºC, the absence of inhibition growth zones surrounding the testing paper discs containing both the effluent and the treated water samples was observed. These qualitative results reveal that both selected microorganisms are resistant to the effluent, either before or after treatment by CWPO, suggesting that the toxicity of the liquid effluent from the MBT plant is not increased during its treatment by CWPO under the optimum operating conditions determined in Section 3.4.1.

3.4.3. Reusability cycles implementing in-situ magnetic separation for catalyst recovery

Catalyst separation and long-term stability are crucial aspects for the feasibility of the proposed water treatment process in large scale applications. Therefore, once the catalytic system and the CWPO process were optimized, the benefits of magnetic separation for the recovery of the catalyst were explored by performing a series of five CWPO reaction/separation sequential experiments in the same vessel with consecutive reuse of the $CoFe_2O_4$/MGNC catalyst, as depicted in Figure 8. For that purpose, the in-situ magnetic separation system developed in Section 3.3 was employed for catalyst recovery at the end of each CWPO cycle, the treated water being collected afterwards. In order to ensure equal catalyst dosage throughout

all the reusability cycles (0.5 g L^{-1}), 23 wt.% of the initial catalyst load was added (i.e., 0.115 g L^{-1}; corresponding to the mass fraction lost due to sampling and treated water collection), and a new CWPO run was performed upon the addition of fresh liquid effluent. As observed in Figure 9, the efficiency of CWPO for the treatment of the liquid effluent from the MBT plant is maintained throughout the five cycles performed in the presence of $CoFe_2O_4$/MGNC under the optimum operating conditions determined in Section 3.4.1. Under these conditions, the COD, TOC, aromaticity and H_2O_2 conversions obtained after 24 h of reaction with $CoFe_2O_4$/MGNC are not particularly affected by the successive reuse of the catalyst, thus revealing its high stability for CWPO, and high potential for large scale applications. This stability feature for CWPO can be ascribed to the resistance of the $CoFe_2O_4$/MGNC catalyst against the leaching of Fe species – which is typically the main cause of catalyst deactivation [8, 14], as highlighted by measuring the dissolved Fe content at the end of each CWPO cycle. Specifically, the highest value was obtained in the first cycle, corresponding to 0.27 mg L^{-1}. From the second to the fifth cycle, the dissolved Fe content was in the range 0.13 – 0.17 mg L^{-1}, the lowest value being obtained after the fifth cycle. The dissolved Fe content obtained after the fifth CWPO cycle is similar to the dissolved Fe content inherent to the liquid effluent (0.15 mg L^{-1}; as discussed in Section 3.4.1), confirming the high resistance of the $CoFe_2O_4$/MGNC catalyst to the leaching of Fe species. Regarding the leaching of Co species, the lowest value was obtained in the first CWPO cycle (0.58 mg L^{-1}), while the highest value was obtained in the third cycle (4.55 mg L^{-1}). The leaching of Co species in the remaining cycles was in the range 1.92 – 2.64 mg L^{-1}, the lowest value being obtained after the fifth cycle. These results suggest that Co species are more susceptible to undergo leaching from the catalyst to the treated waters than Fe species, which is in line with the results previously reported on the application of bimetallic iron-cobalt magnetic carbon xerogels in CWPO [38].

FIGURE 8

FIGURE 9

4. Conclusions

All the hybrid magnetic graphitic nanocomposites developed in this work revealed catalytic activity in the CWPO of 4-NP. Nevertheless, the best performance was achieved with the material resulting from the inclusion of $CoFe_2O_4$ into a graphitic structure during the synthesis of $CoFe_2O_4$/MGNC.

The efficiency of CWPO for the treatment of the effluent from a MBT plant was strongly influenced by the operating pH, a phenomenon which was ascribed to the presence of bicarbonates and chlorides. At pH > 6, H_2O_2 is readily consumed due to the fast reaction with HCO_3^-; while at pH < 6, the $HO^{\bullet}$ radical scavenging by Cl^- hinders the efficiency of the CWPO process. Based on the COD, TOC, H_2O_2 and aromaticity conversions obtained, pH = 6 was considered the optimum operating pH for the liquid effluent treatment by CWPO in the presence of $CoFe_2O_4$/MGNC. The biodegradability of the liquid effluent was enhanced during the treatment, as reflected by the 2-fold increase of the BOD_5/COD ratio obtained. In addition, disinfection of the liquid effluent was achieved and the treated water revealed no toxicity against selected bacteria.

A magnetic separation system was developed for the in-situ recovery of the $CoFe_2O_4$/MGNC catalyst after the CWPO reaction stage. The high stability of $CoFe_2O_4$/MGNC for the CWPO of the liquid effluent considered in this work was demonstrated by performing a series of five CWPO reaction/separation sequential experiments in the same vessel.

The ability of the developed catalytic system to enable the treatment of the liquid effluent from a MBT plant for MSW by CWPO – in spite of its very high concentration of chlorides and bicarbonates, and in a wide range of operating pH – opens future prospects for the applicability of this wastewater treatment technology.

Acknowledgments

This work was financially supported by: Project POCI-01-0145-FEDER-006984 – Associate Laboratory LSRE-LCM funded by FEDER through COMPETE2020 - Programa Operacional Competitividade e Internacionalização (POCI) – and by national funds through FCT - Fundação para a Ciência e a Tecnologia; Project VALORCOMP, funded by FEDER through Programme INTERREG V-A Spain – Portugal (POCTEP) 2014-2020. R.S. Ribeiro and R.O. Rodrigues acknowledge the FCT individual Ph.D. grants SFRH/BD/94177/2013 and SFRH/BD/97658/2013, respectively, with financing from FCT and the European Social Fund (through POPH and QREN). A.M.T. Silva acknowledges the FCT Investigator 2013 Programme (IF/01501/2013), with financing from the European Social Fund and the Human Potential Operational Programme.

References

[1] A. Cesaro, L. Russo, A. Farina, V. Belgiorno, Organic fraction of municipal solid waste from mechanical selection: biological stabilization and recovery options, Environ. Sci. Pollut. Res. 23 (2016) 1565-1575.

[2] H. Shahriari, M. Warith, M. Hamoda, K.J. Kennedy, Anaerobic digestion of organic fraction of municipal solid waste combining two pretreatment modalities, high temperature microwave and hydrogen peroxide, Waste Manage. 32 (2012) 41-52.

[3] Council Directive 99/31/EC of 26 April 1999 on the landfill of waste, Official Journal of the European Communities, The Council of the European Union, 1999.

[4] M. Ragazzi, P. Tosi, E.C. Rada, V. Torretta, M. Schiavon, Effluents from MBT plants: Plasma techniques for the treatment of VOCs, Waste Manage. 34 (2014) 2400-2406.

[5] J. Fang, H. Zhang, N. Yang, L. Shao, P. He, Gaseous pollutants emitted from a mechanical biological treatment plant for municipal solid waste: Odor assessment and photochemical reactivity, J. Air Waste Manage. Assoc. 63 (2013) 1287-1297.

[6] Mechanical biological treatment of municipal solid waste, Department for Environment, Food & Rural Affairs, London, 2013.

[7] D. Weichgrebe, S. Maerker, T. Böning, H. Stegemann, Intended process water management concept for the mechanical biological treatment of municipal solid waste, Water Sci. Eng. 1 (2008) 78-88.

[8] M. Munoz, Z.M. de Pedro, J.A. Casas, J.J. Rodriguez, Preparation of magnetite-based catalysts and their application in heterogeneous Fenton oxidation – A review, Appl. Catal., B 176–177 (2015) 249-265.

[9] R.S. Ribeiro, A.M.T. Silva, P.B. Tavares, J.L. Figueiredo, J.L. Faria, H.T. Gomes, Hybrid magnetic graphitic nanocomposites for catalytic wet peroxide oxidation applications, Catal. Today 280 (2017) 184-191.

[10] C.M. Domínguez, A. Quintanilla, J.A. Casas, J.J. Rodríguez, Treatment of real winery wastewater by wet oxidation at mild temperature, Sep. Purif. Technol. 129 (2014) 121-128.

[11] Y. Yan, S. Jiang, H. Zhang, Efficient catalytic wet peroxide oxidation of phenol over Fe-ZSM-5 catalyst in a fixed bed reactor, Sep. Purif. Technol. 133 (2014) 365-374.

[12] P.R. Gogate, A.B. Pandit, A review of imperative technologies for wastewater treatment I: oxidation technologies at ambient conditions, Adv. Environ. Res. 8 (2004) 501-551.

[13] S. Navalon, M. Alvaro, H. Garcia, Heterogeneous Fenton catalysts based on clays, silicas and zeolites, Appl. Catal., B 99 (2010) 1-26.

[14] R.S. Ribeiro, A.M.T. Silva, J.L. Figueiredo, J.L. Faria, H.T. Gomes, Catalytic wet peroxide oxidation: a route towards the application of hybrid magnetic carbon nanocomposites for the degradation of organic pollutants. A review, Appl. Catal., B 187 (2016) 428-460.

[15] P.V. Nidheesh, Heterogeneous Fenton catalysts for the abatement of organic pollutants from aqueous solution: a review, RSC Adv. 5 (2015) 40552-40577.

[16] M. Muruganandham, R.P.S. Suri, M. Sillanpää, J.J. Wu, B. Ahmmad, S. Balachandran, M. Swaminathan, Recent developments in heterogeneous catalyzed environmental remediation processes, J. Nanosci. Nanotechnol. 14 (2014) 1898-1910.

[17] S. Rahim Pouran, A.A. Abdul Raman, W.M.A. Wan Daud, Review on the application of modified iron oxides as heterogeneous catalysts in Fenton reactions, J. Cleaner Prod. 64 (2014) 24-35.

[18] M.C. Pereira, L.C.A. Oliveira, E. Murad, Iron oxide catalysts: Fenton and Fenton-like reactions - A review, Clay Miner. 47 (2012) 285-302.

[19] A. Dhakshinamoorthy, S. Navalon, M. Alvaro, H. Garcia, Metal nanoparticles as heterogeneous Fenton catalysts, ChemSusChem 5 (2012) 46-64.

[20] S. Navalon, A. Dhakshinamoorthy, M. Alvaro, H. Garcia, Heterogeneous Fenton catalysts based on activated carbon and related materials, ChemSusChem 4 (2011) 1712-1730.

[21] P.V. Nidheesh, R. Gandhimathi, S.T. Ramesh, Degradation of dyes from aqueous solution by Fenton processes: a review, Environ. Sci. Pollut. Res. 20 (2013) 2099-2132.

[22] Y. Zhang, Z. Yang, D. Yin, Y. Liu, C. Fei, R. Xiong, J. Shi, G. Yan, Composition and magnetic properties of cobalt ferrite nano-particles prepared by the co-precipitation method, J. Magn. Magn. Mater. 322 (2010) 3470-3475.

[23] K. Maaz, S. Karim, A. Mumtaz, S.K. Hasanain, J. Liu, J.L. Duan, Synthesis and magnetic characterization of nickel ferrite nanoparticles prepared by co-precipitation route, J. Magn. Magn. Mater. 321 (2009) 1838-1842.

[24] R.S. Ribeiro, Z. Frontistis, D. Mantzavinos, D. Venieri, M. Antonopoulou, I. Konstantinou, A.M.T. Silva, J.L. Faria, H.T. Gomes, Magnetic carbon xerogels for the catalytic wet peroxide oxidation of sulfamethoxazole in environmentally relevant water matrices, Appl. Catal., B 199 (2016) 170-186.

[25] A. Aguinaco, J.P. Pocostales, J.F. García-Araya, F.J. Beltrán, Decomposition of hydrogen peroxide in the presence of activated carbons with different characteristics, J. Chem. Technol. Biotechnol. 86 (2011) 595-600.

[26] R.S. Ribeiro, A.M.T. Silva, L.M. Pastrana-Martínez, J.L. Figueiredo, J.L. Faria, H.T. Gomes, Graphene-based materials for the catalytic wet peroxide oxidation of highly concentrated 4-nitrophenol solutions, Catal. Today 249 (2015) 204–212.

[27] L.S. Clescerl, A.E. Greenberg, A.D. Eaton, Standard methods for the examination of water and wastewater, twentieth ed., American Public Health Association, American Water Works Association, Water Environment Federation, Washington DC, 1999.

[28] Y.W. Kang, M.-J. Cho, K.-Y. Hwang, Correction of hydrogen peroxide interference on standard chemical oxygen demand test, Water Res. 33 (1999) 1247-1251.

[29] M. Mrkva, Evaluation of correlations between absorbance at 254 nm and COD of river waters, Water Res. 17 (1983) 231-235.

[30] ISO 6332:1988, Water quality - Determination of iron - Spectrometric method using 1,10-phenanthroline, International Organization for Standardization, 1988.

[31] G. Tchobanoglous, F.L. Burton, H.D. Stensel, Wastewater engineering: treatment and reuse, fourth ed., International Edition, Metcalf & Eddy, Inc., McGraw-Hill companies, New York, 2003.

[32] M. Balouiri, M. Sadiki, S.K. Ibnsouda, Methods for in vitro evaluating antimicrobial activity: A review, J. Pharm. Anal. 6 (2016) 71-79.

[33] L.E. Lagoeiro, Transformation of magnetite to hematite and its influence on the dissolution of iron oxide minerals, J. Metamorph. Geol. 16 (1998) 415-423.

[34] A. Jafari, S. Farjami Shayesteh, M. Salouti, K. Boustani, Effect of annealing temperature on magnetic phase transition in Fe_3O_4 nanoparticles, J. Magn. Magn. Mater. 379 (2015) 305-312.

[35] R. Liu, L. Wan, S. Liu, Y. Yu, S. Li, D. Wu, Hierarchical co-assembly avenue to uniform rhombododecahedral magnetic mesoporous graphitic composites, J. Colloid Interface Sci. 414 (2014) 59-65.

[36] M. Kosmulski, The pH dependent surface charging and points of zero charge. VI. Update, J. Colloid Interface Sci. 426 (2014) 209-212.

[37] M. Kosmulski, pH-dependent surface charging and points of zero charge. IV. Update and new approach, J. Colloid Interface Sci. 337 (2009) 439-448.

[38] R.S. Ribeiro, A.M.T. Silva, J.L. Figueiredo, J.L. Faria, H.T. Gomes, The role of cobalt in bimetallic iron-cobalt magnetic carbon xerogels developed for catalytic wet peroxide oxidation, Catal. Today (2017), DOI: 10.1016/j.cattod.2017.1006.1023.

[39] E.P. Agency, Parameters of water quality: Interpretation and standards, Environmental Protection Agency, Ireland, Wexford, Ireland, 2001.

[40] S. Parsons, Advanced oxidation processes for water and wastewater treatment, IWA Publishing, London, UK, 2004.

[41] J. De Laat, T.G. Le, Effects of chloride ions on the iron(III)-catalyzed decomposition of hydrogen peroxide and on the efficiency of the Fenton-like oxidation process, Appl. Catal., B 66 (2006) 137-146.

[42] D.R. Lide, CRC Handbook of Chemistry and Physics, eighty fourth ed., CRC Press, Boca Raton, 2003.

[43] F.K. Attiogbe, W. Wang, A. McNeillie, R.C. Francis, The peroxymonocarbonate anions as pulp bleaching agents. Part 2. Mechanical pulp brightening and effects of metal ions, Bioresources 5 (2010) 2221-2231.

[44] C.H. Atwood, Survival guide for introductory chemistry, first ed., Brooks/Cole Cengage Learning, Belmont, CA, 2009.

[45] C.-H. Liao, S.-F. Kang, F.-A. Wu, Hydroxyl radical scavenging role of chloride and bicarbonate ions in the H_2O_2/UV process, Chemosphere 44 (2001) 1193-1200.

[46] M.J. Allen, S.C. Edberg, D.J. Reasoner, Heterotrophic plate count bacteria - what is their significance in drinking water?, Int. J. Food Microbiol. 92 (2004) 265-274.

[47] J. Bartram, J. Cotruvo, M. Exner, C. Fricker, A. Glasmacher, Heterotrophic plate counts and drinking-water safety: the significance of HPCs for water quality and the human health, Published on behalf of World Health Organization (WHO) by IWA Publishing, London, 2003.

[48] D.J. Reasoner, Heterotrophic plate count methodology in the United States, Int. J. Food Microbiol. 92 (2004) 307-315.

TABLES

Table 1. Characterization of the liquid effluent from the MBT plant for MSW located in Northern Portugal, as determined in triplicate measurements

Parameter	Value	Units
Chemical oxygen demand (COD)	9206 ± 284	mg L^{-1}
Biochemical oxygen demand (BOD_5)	1933 ± 153	mg L^{-1}
Total organic carbon (TOC)	2046 ± 16	mg L^{-1}
Chlorides	2833 ± 14	mg L^{-1}
pH at 25 ºC	8.20 ± 0.01	Sørensen scale
Total Fe content	6.4 ± 0.1	mg L^{-1}
Dissolved Co content	0.12 ± 0.01	mg L^{-1}
Total heterotrophic bacteria cultivable at 28 ºC	14.7 ± 2.1	× 10^4 CFU mL^{-1}
Conductivity[a]	23933 ± 4554	µS cm^{-1}
Bicarbonates[a]	14350 ± 50	mg L^{-1}
Ammonia nitrogen[a]	2300 ± 285	mg L^{-1}
Total hydrocarbons[a]	4 ± 1	mg L^{-1}

[a] As determined in quarterly analysis provided by the intermunicipal company.

Table 2. Properties of the MGNC materials: specific surface area (S_{BET}), non-microporous specific surface area (S_{meso}), micropore volume (V_{micro}), total pore volume (V_{total}), average pore diameter (d_{pore}) and pH at the point of zero charge (pH_{PZC})

Material	Parameter					
	S_{BET} (m^2 g^{-1})	S_{meso} (m^2 g^{-1})	V_{mic} (cm^3 g^{-1})	V_{total} (cm^3 g^{-1})	d_{pore} (nm)	pH_{PZC}
Fe_3O_4/MGNC	330	170	0.07	0.31	3.75	7.1
$NiFe_2O_4$/MGNC	345	135	0.10	0.29	3.36	8.7
$CoFe_2O_4$/MGNC	330	170	0.07	0.31	3.75	9.0

FIGURE CAPTIONS

Figure 1. XRD diffraction patterns of (a) Fe_3O_4 and Fe_3O_4/MGNC, (b) $NiFe_2O_4$ and $NiFe_2O_4$/MGNC, and (c) $CoFe_2O_4$ and $CoFe_2O_4$/MGNC. Standard reference patterns of magnetite (crystallography open database code: 9005840), nickel ferrite (crystallography open database code: 2300289) and cobalt ferrite (crystallography open database code: 1535820) are also given for comparison.

Figure 2. TEM micrographs: (main) of (a) Fe_3O_4/MGNC, (c) $NiFe_2O_4$/MGNC and (e) $CoFe_2O_4$/MGNC; and (inset) of (a) Fe_3O_4, (c) $NiFe_2O_4$ and (e) $CoFe_2O_4$. Histogram of particle size distribution: (main) of the metal core of (b) Fe_3O_4/MGNC, (d) $NiFe_2O_4$/MGNC and (f) $CoFe_2O_4$/MGNC; and (inset) of (b) Fe_3O_4, (d) $NiFe_2O_4$ and (f) $CoFe_2O_4$, as determined by TEM measurements.

Figure 3. 4-NP and H_2O_2 conversions obtained as a function of time in CWPO runs performed with the MGNC materials. Experiments performed with $[4\text{-NP}]_0 = 5$ g L^{-1}, [catalyst] = 0.5 g L^{-1}, $T = 80$ °C, pH = 3 and $[H_2O_2]_0 = [H_2O_2]_{Stoichiometric} = 17.8$ g L^{-1}.

Figure 4. (a) 4-NP, COD, TOC and H_2O_2 conversions as a function of time in the CWPO run performed with $CoFe_2O_4$/MGNC; 4-NP removals by adsorption are also shown for comparison. (b) 4-NP and TOC removals obtained during the "leaching test" performed with $CoFe_2O_4$/MGNC (i.e. where the catalyst was removed from the solution after 30 min of reaction). (c) Effect of *tert*-butanol (tBuOH) on the CWPO removal of 4-NP when using $CoFe_2O_4$/MGNC. Experiments performed under the conditions given in Figure 3.

Figure 5. Evolution of aromatic (a) and non-aromatic (b) by-products of 4-NP oxidation, when using $CoFe_2O_4$/MGNC in the CWPO process developed under the conditions given in Figure 3.

Figure 6. in-situ magnetic separation of $CoFe_2O_4$/MGNC at the end of the CWPO stage performed with the aid of a Mitutoyo 7033B switchable magnetic stand (clamping force 600

N); (a) front and (b) top view of the glass reactor immediately after the recovery of the treated water and (c) top view of the reactor after the drying process (60 ºC) for catalyst recovery.

Figure 7. (a) Effect of pH on COD, TOC, H_2O_2 and aromaticity conversions obtained after 24 h in CWPO runs performed with $CoFe_2O_4$/MGNC. (b) COD, TOC, H_2O_2, aromaticity [left axis], solution pH [right axis] and (c) absorbance spectra evolution as a function of time in the CWPO run performed at pH 6; Experiments performed with the liquid effluent collected from a MBT plant, [$CoFe_2O_4$/MGNC] = 0.5 g L^{-1}, T = 80 ºC, pH = 6 and $[H_2O_2]_0$ = 27.7 g L^{-1}.

Figure 8. Experimental procedure during the CWPO reusability cycles performed with the liquid effluent collected from a MBT plant and $CoFe_2O_4$/MGNC.

Figure 9. COD, TOC, H_2O_2 and aromaticity conversions obtained after 24 h in a series of five CWPO runs performed with consecutive reuse of $CoFe_2O_4$/MGNC. Experiments performed with the liquid effluent collected from a MBT plant, [$CoFe_2O_4$/MGNC] = 0.5 g L^{-1}, T = 80 ºC, pH = 6 and $[H_2O_2]_0$ = 27.7 g L^{-1}.

FIGURE 1

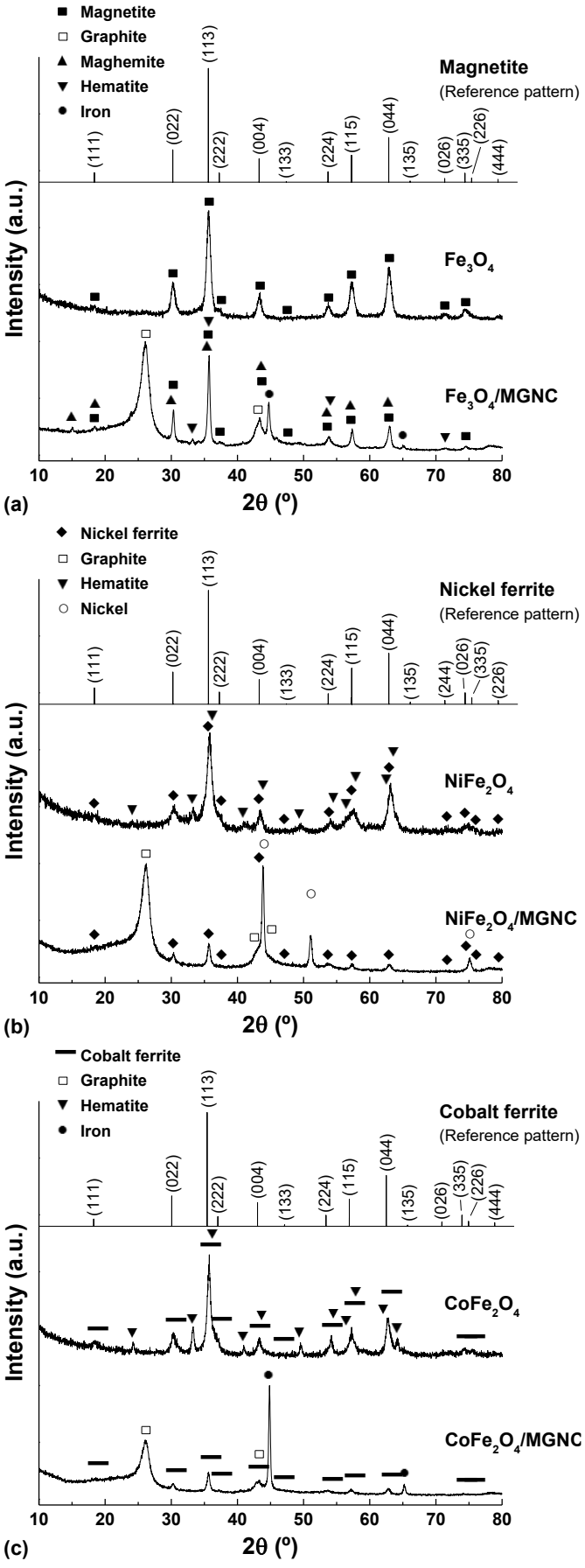
Magnetite
Graphite
Maghemite
Hematite
Iron
Magnetite
(Reference pattern)
(111)
(022)
(113)
(222)
(004)
(133)
(224)
(115)
(044)
(135)
(026)
(335)
(226)
(444)
Intensity (a.u.)
Fe3O4
Fe3O4/MGNC
10
20
30
40
50
60
70
80
(a)
2θ (º)
Nickel ferrite
Graphite
Hematite
Nickel
Nickel ferrite
(Reference pattern)
(111)
(022)
(113)
(222)
(004)
(133)
(224)
(115)
(044)
(135)
(244)
(026)
(335)
(226)
Intensity (a.u.)
NiFe2O4
NiFe2O4/MGNC
10
20
30
40
50
60
70
80
(b)
2θ (º)
Cobalt ferrite
Graphite
Hematite
Iron
Cobalt ferrite
(Reference pattern)
(111)
(022)
(113)
(222)
(004)
(133)
(224)
(115)
(044)
(135)
(026)
(335)
(226)
(444)
Intensity (a.u.)
CoFe2O4
CoFe2O4/MGNC
10
20
30
40
50
60
70
80
(c)
2θ (º)

FIGURE 2

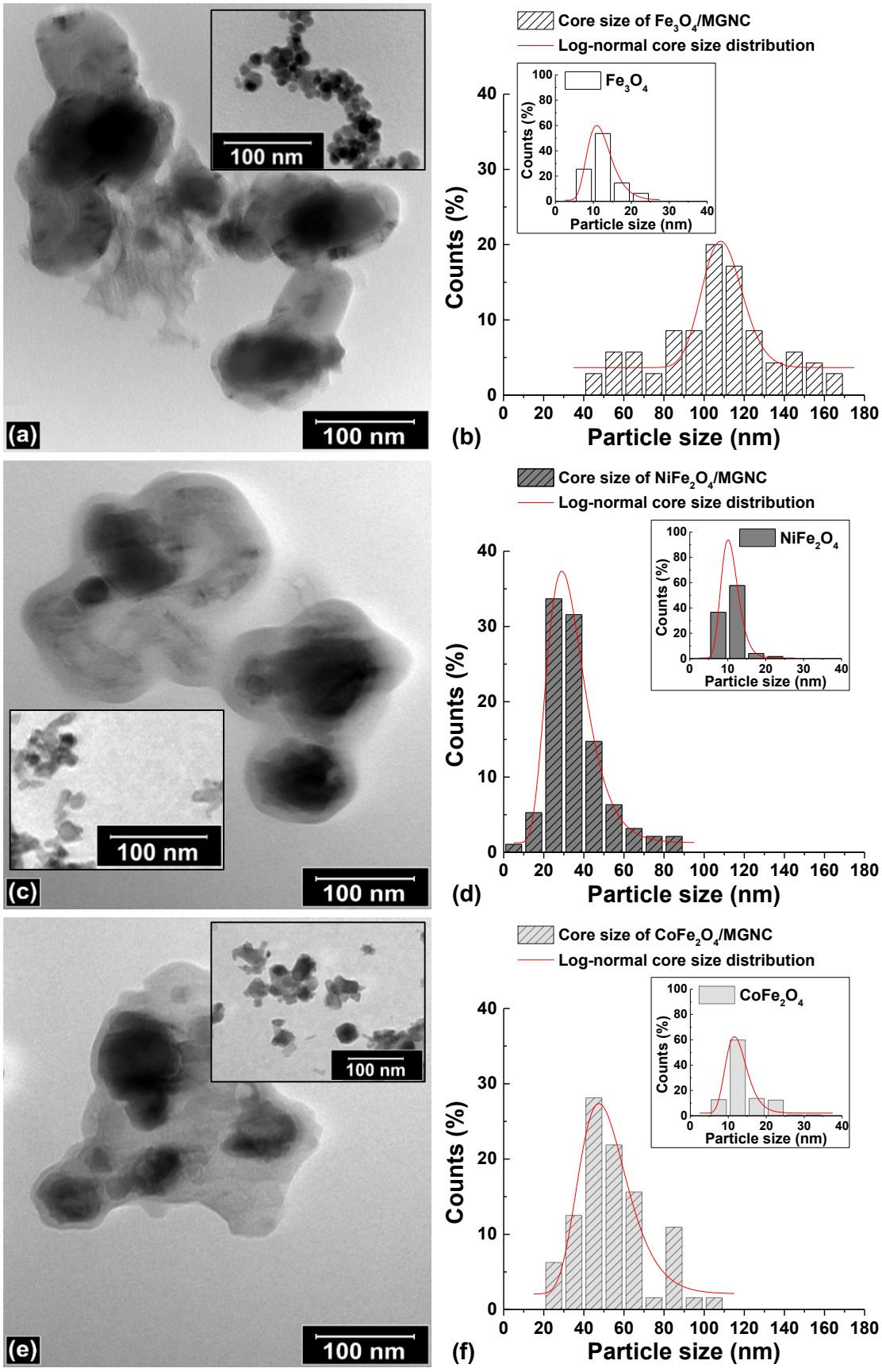
100 nm
(a)
100 nm
Core size of Fe_3O_4/MGNC
Log-normal core size distribution
Fe_3O_4
Counts (%)
Particle size (nm)
(b)
Particle size (nm)
100 nm
(c)
100 nm
Core size of $NiFe_2O_4$/MGNC
Log-normal core size distribution
$NiFe_2O_4$
Counts (%)
Particle size (nm)
(d)
Particle size (nm)
100 nm
(e)
100 nm
Core size of $CoFe_2O_4$/MGNC
Log-normal core size distribution
$CoFe_2O_4$
Counts (%)
Particle size (nm)
(f)
Particle size (nm)

FIGURE 3

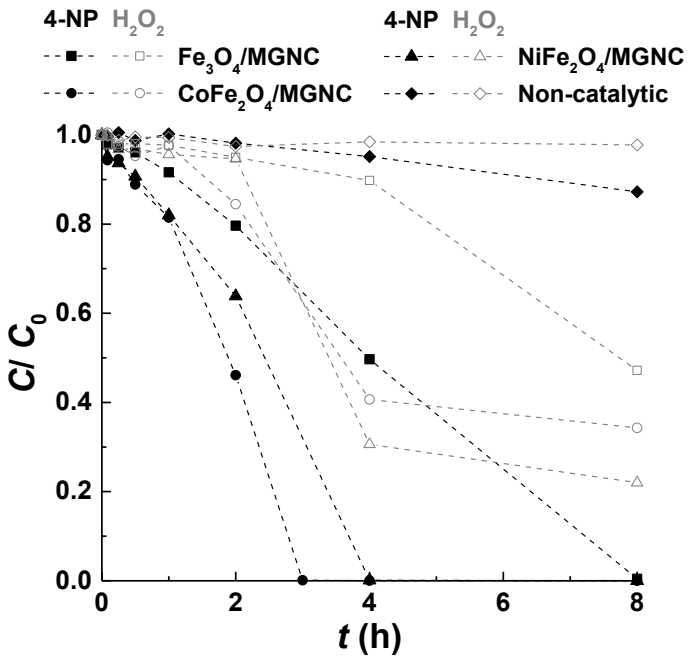
4-NP H2O2
Fe3O4/MGNC
CoFe2O4/MGNC
4-NP H2O2
NiFe2O4/MGNC
Non-catalytic
C/ C0
t (h)
1.0
0.8
0.6
0.4
0.2
0.0
0
2
4
6
8

FIGURE 4

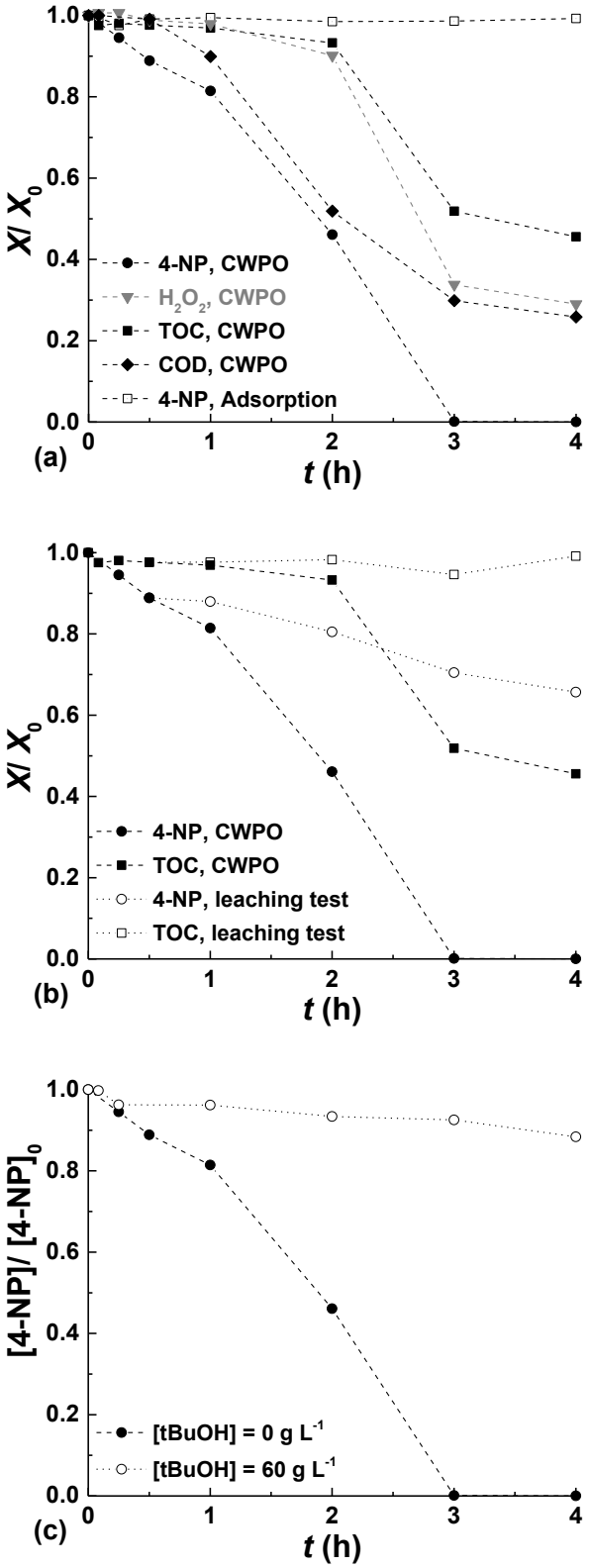
X/ X0
4-NP, CWPO
H2O2, CWPO
TOC, CWPO
COD, CWPO
4-NP, Adsorption
(a)
t (h)
X/ X0
4-NP, CWPO
TOC, CWPO
4-NP, leaching test
TOC, leaching test
(b)
t (h)
[4-NP]/ [4-NP]0
[tBuOH] = 0 g L-1
[tBuOH] = 60 g L-1
(c)
t (h)

FIGURE 5

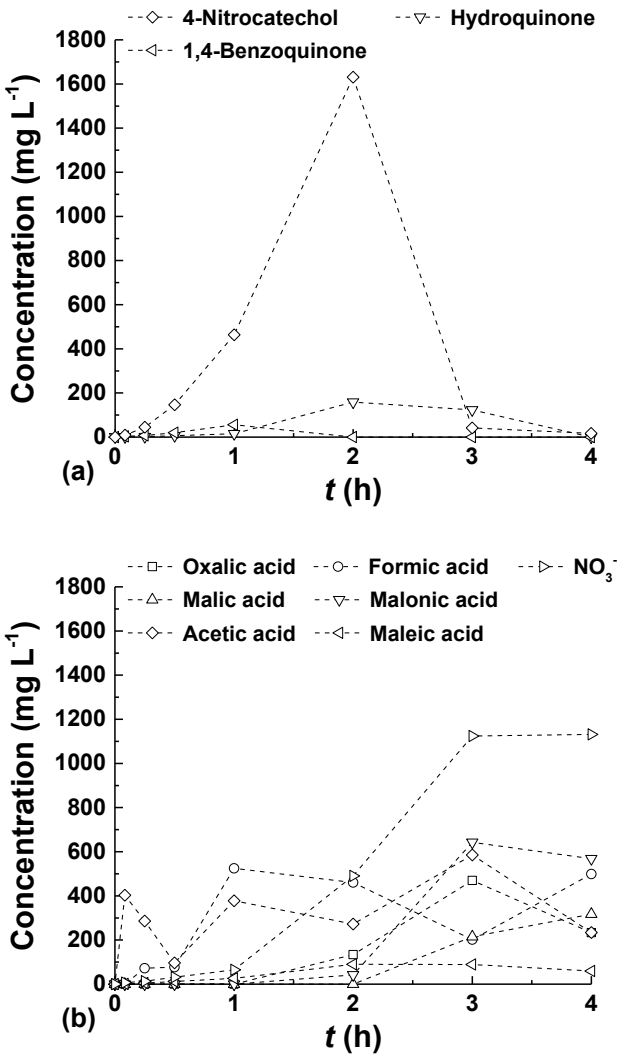
4-Nitrocatechol
Hydroquinone
1,4-Benzoquinone
Concentration (mg L-1)
t (h)
(a)
Oxalic acid
Formic acid
NO3-
Malic acid
Malonic acid
Acetic acid
Maleic acid
Concentration (mg L-1)
t (h)
(b)

FIGURE 6

(a) 

(b) 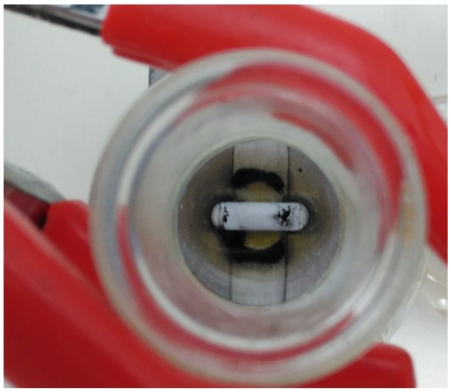

(c) 

FIGURE 7

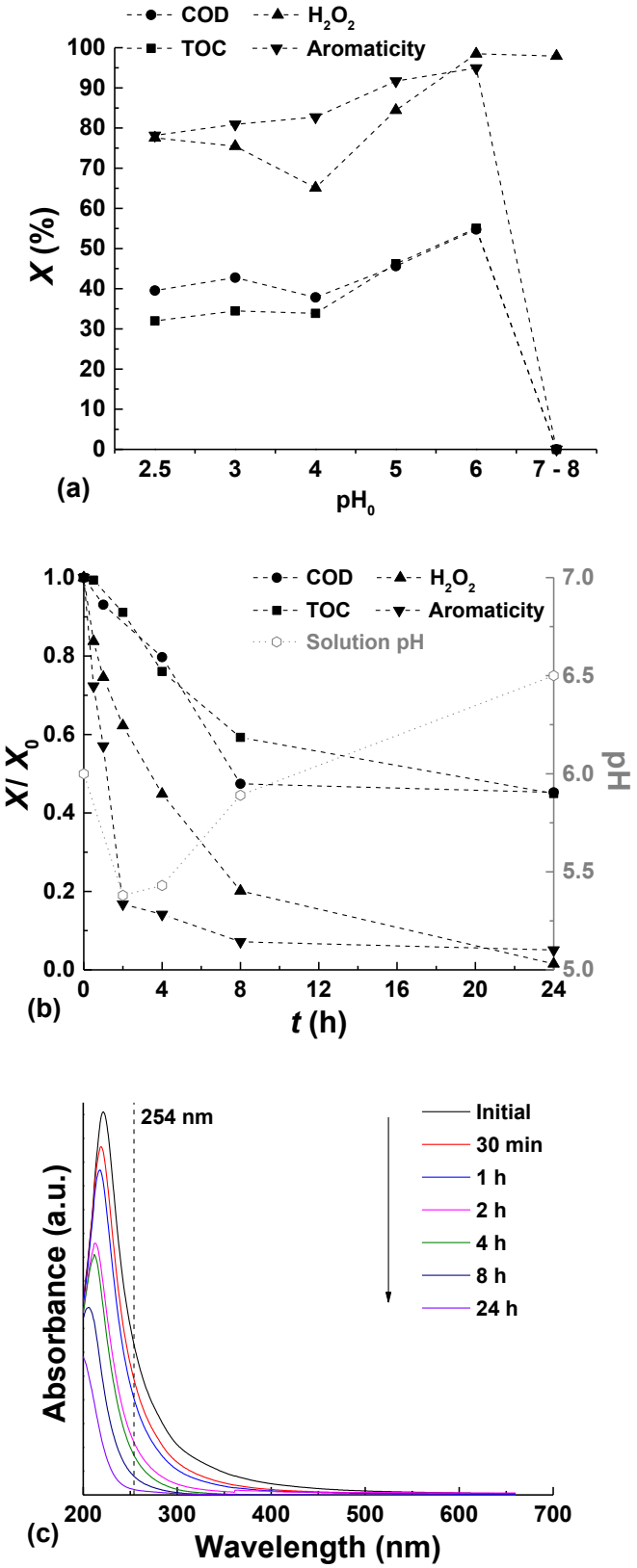
COD
H2O2
TOC
Aromaticity
X (%)
pH0
(a)
Solution pH
X/ X0
pH
t (h)
(b)
254 nm
Initial
30 min
1 h
2 h
4 h
8 h
24 h
Absorbance (a.u.)
Wavelength (nm)
(c)

FIGURE 8

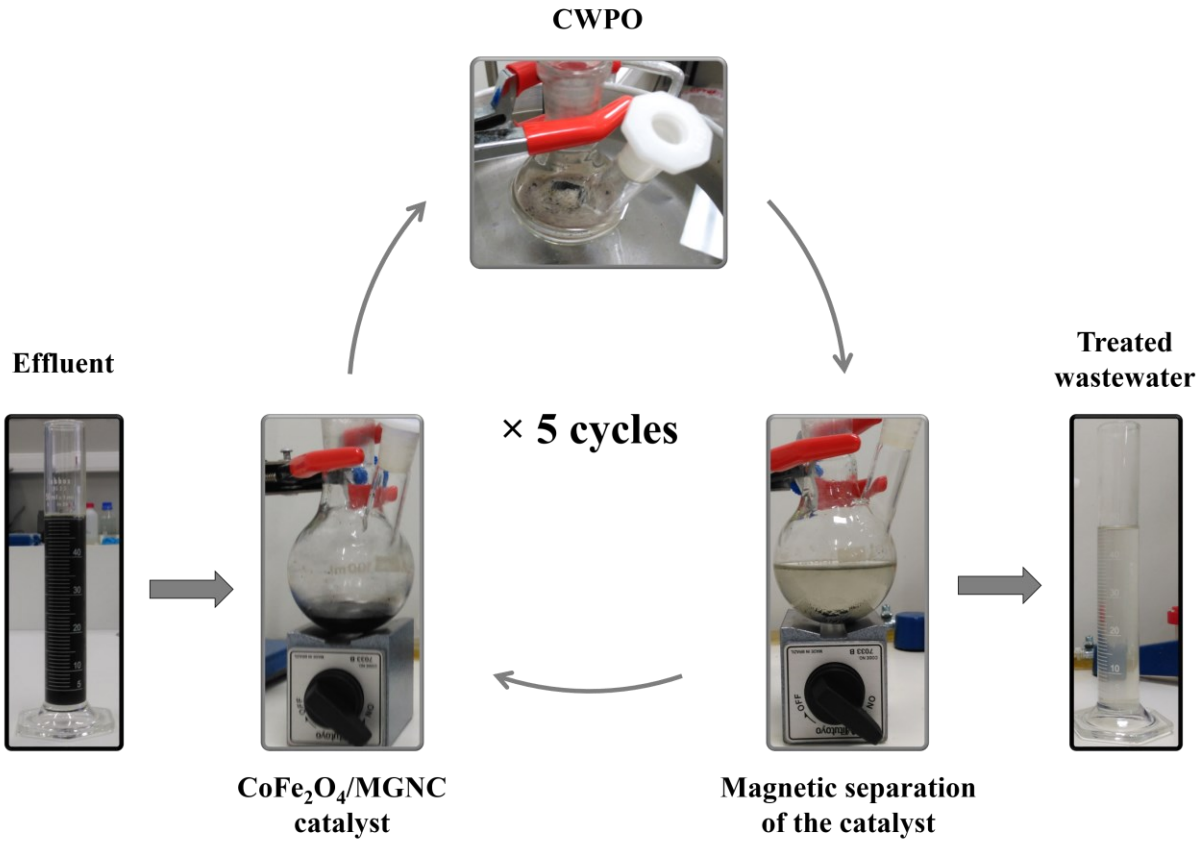
CWPO
Effluent
Treated wastewater
× 5 cycles
$CoFe_2O_4$/MGNC catalyst
Magnetic separation of the catalyst

FIGURE 9

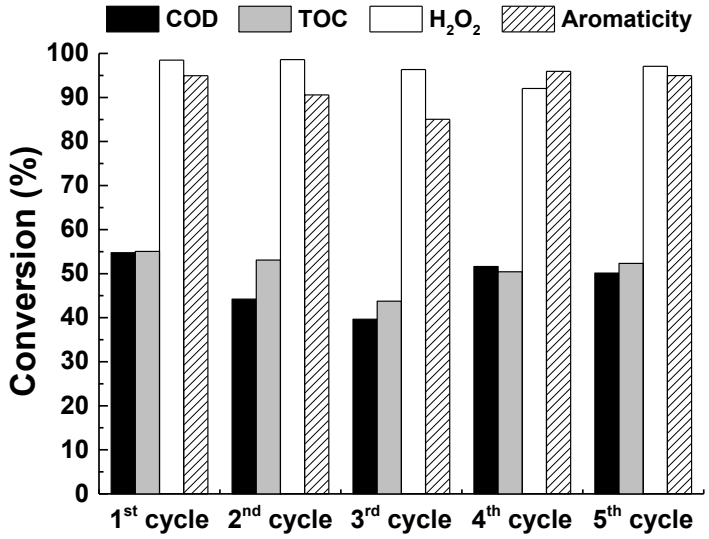
COD
TOC
H2O2
Aromaticity
Conversion (%)
100
90
80
70
60
50
40
30
20
10
0
1st cycle
2nd cycle
3rd cycle
4th cycle
5th cycle